energies

MDPI

Article

Research on the Production of Turquoise Hydrogen from Methane (CH_4) through Plasma Reaction

Dong-Kyoo Park, Soo-Nam Park, Hyun-Ji Kim, Hyo-Sik Kim, Ji-Hyeon Kim and Jae-Hong Ryu *

Institute for Advanced Engineering, Yongin 41718, Republic of Korea; parkdk@iae.re.kr (D.-K.P.); trackerdog@iae.re.kr (S.-N.P.); hj.kim@iae.re.kr (H.-J.K.); hyosgogo@iae.re.kr (H.-S.K.); kimjyun@iae.re.kr (J.-H.K.)
* Correspondence: jhryu@iae.re.kr; Tel.: +82-31-330-7882

Abstract: Turquoise hydrogen is produced through a process of separating carbon into solid carbon based on fossil fuels and refers to hydrogen that does not produce carbon dioxide. In this study, the characteristics of turquoise hydrogen production through a methane thermal cracking reaction using an arc plasma torch were investigated. The plasma torch operated stably under high voltage and transport gas flow conditions. The composition of the gas generated from the methane plasma reaction was analyzed using an online IR gas analyzer and GC-FID. The experimental results show that the hydrogen yield decreased to 16.4% as the methane feed rate increased but increased to 58.8% as the plasma power increased. Under these conditions, the yield of solid carbon, a valuable byproduct, was also shown to increase to 62.9%. In addition, solid carbon showed high-temperature heat-treated characteristics based on its generation location. Carbon oxides such as CO and CO_2 are rarely generated under any experimental conditions. Consequently, it can be considered that plasma thermal cracking is a promising technology for CO_2-free hydrogen production and a valuable solid carbon.

Keywords: turquoise H_2; plasma; thermal cracking; methane; solid carbon

check for updates

Citation: Park, D.-K.; Park, S.-N.; Kim, H.-J.; Kim, H.-S.; Kim, J.-H.; Ryu, J.-H. Research on the Production of Turquoise Hydrogen from Methane (CH_4) through Plasma Reaction. *Energies* **2024**, *17*, 484. https://doi.org/10.3390/en17020484

Academic Editor: Jinliang Yuan

Received: 23 December 2023
Revised: 15 January 2024
Accepted: 16 January 2024
Published: 19 January 2024

Copyright: © 2024 by the authors. Licensee MDPI, Basel, Switzerland. This article is an open access article distributed under the terms and conditions of the Creative Commons Attribution (CC BY) license (https://creativecommons.org/licenses/by/4.0/).

1. Introduction

Human activities lead to the emission and generation of greenhouse gases. The removal of already-emitted greenhouse gases can be achieved through methods such as forest absorption or carbon capture utilization and storage (CCUS). The goal is to reduce current greenhouse gas emissions to zero. Carbon neutrality became a hot topic in the international community in 2018 when the United Nations Intergovernmental Panel on Climate Change (IPCC) stated in its "Global Warming 1.5 °C special report" that the global temperature should not rise more than 1.5 °C [1].

A lot of effort is being made to achieve carbon neutrality around the world, and Korea has also recently been sequentially pursuing related policies to achieve carbon neutrality. Hydrogen is attracting attention as a technology that can achieve carbon neutrality because it is environmentally friendly.

Hydrogen has the advantage of being a clean fuel that can be used as an energy storage medium. So far, global hydrogen production has been carried out using the cost-competitive steam methane-reforming (SMR) method, but this has been accompanied by high emissions of carbon dioxide and consumption of fossil resources. Eco-friendly hydrogen production technology through water electrolysis using electricity obtained from renewable energy is an attractive technology but is not widely available due to low price competitiveness.

As a measure of greenhouse gases, gray, green, blue, and turquoise color codes have been assigned to hydrogen production technology by the IEA, and there is a lot of interest in green hydrogen and turquoise hydrogen as clean hydrogen [2,3].

Byproduct hydrogen and reformed hydrogen are classified as gray hydrogen. Be-cause byproduct hydrogen is generated incidentally in petrochemical and steel manufacturing

processes, there are limits to increasing production. Reformed hydrogen using natural gas has the advantage of being able to be mass-produced, but it has been pointed out that a large amount of carbon dioxide is produced as a byproduct.

Blue hydrogen is what complements the limitations of gray hydrogen. The production method is the same as that of gray hydrogen, but it is called clean hydrogen because the carbon dioxide generated during the production process is removed using CCUS technology. The captured carbon dioxide is permanently stored or used in cement, semiconductor gas, tire materials, etc. Blue hydrogen has been evaluated as the most realistic alternative for expanding the hydrogen industry.

Green hydrogen is a technology that produces electricity by decomposing water using electricity generated from renewable energy such as solar power or wind power and is attracting attention as the ultimate clean energy because it does not emit carbon dioxide. However, economic and technical limitations must be overcome in order to mass produce green hydrogen, such as using water electrolysis production facilities and renewable energy. In addition, hydrogen produced by decomposing water using the existing power grid rather than renewable energy is called yellow hydrogen, and hydrogen produced by decomposing water using electricity generated through nuclear power generation is called pink hydrogen [4].

Additionally, hydrogen produced by methane pyrolysis is called turquoise hydrogen, and it is potentially one of the most promising technologies in the field of clean hydrogen production. The biggest advantage of this technology is that can decompose methane into hydrogen and solid carbon without using traditional oxidizers. In this case, no carbon oxides are emitted, and the solid carbon can be removed from the reactor and later used as a commercial byproduct. This also eliminates the need for expensive CCS facilities. It is a promising feedstock for hydrogen production, especially since the infrastructure for the production, storage, and transportation of natural gas is sufficiently well developed worldwide.

The direct decomposition of methane into hydrogen and carbon is an endothermic process with a single-stage reaction [5–7].

$$CH_4(g) \rightarrow 2H_2 + C,\ \Delta Ho = 74\ kJ/mol$$

Technological variants of methane pyrolysis are divided into three categories, depending on the predominant method of energy exposure and reaction conditions: thermal decomposition, plasma decomposition, and catalytic decomposition [8].

Among these, one method for methane pyrolysis is to use plasma, and the pyrolysis energy demand is supplied by electricity. Methane decomposes into hydrogen and carbon byproducts through thermal decomposition via plasma discharge. Unlike other pyrolysis process technologies, plasma has a fast start-up, allowing for flexible reactor operation. Hydrogen production can therefore be easily scaled to match the availability of renewable electricity [9–12].

Monolith, a company that commercializes the methane pyrolysis process using a plasma heat source, has been operating since 2012. In 2020, it produced 14,000 tons of black and 2500 tons of hydrogen. Monolith's plasma source relies on technology for the simultaneous production of hydrogen and carbon black based on plasma (2000 °C) using 100% renewable energy in the form of arc discharge [13]

When decomposing hydrocarbons using plasma, a lot of electricity is consumed and the durability of the burner that generates the plasma is short due to the instantaneous high temperature. During plasma discharge, disadvantages of unstable discharge and low conversion of methane arise due to the interference of the methane reaction due to carbon growth as a plasma electrode. Therefore, it is important to design a plasma reactor to overcome these problems.

In this study, we designed and manufactured an arc plasma reactor and confirmed the possibility of a scaled-up design via gas analysis along with the phenomenon of hydrogen and carbon black generation through arc discharge after supplying methane.

2. Materials and Methods

2.1. Plasma Torch and Chamber Reactor

To study the characteristics of methane thermal cracking using plasma, a plasma torch and chamber reactor were manufactured, as shown in Figure 1.

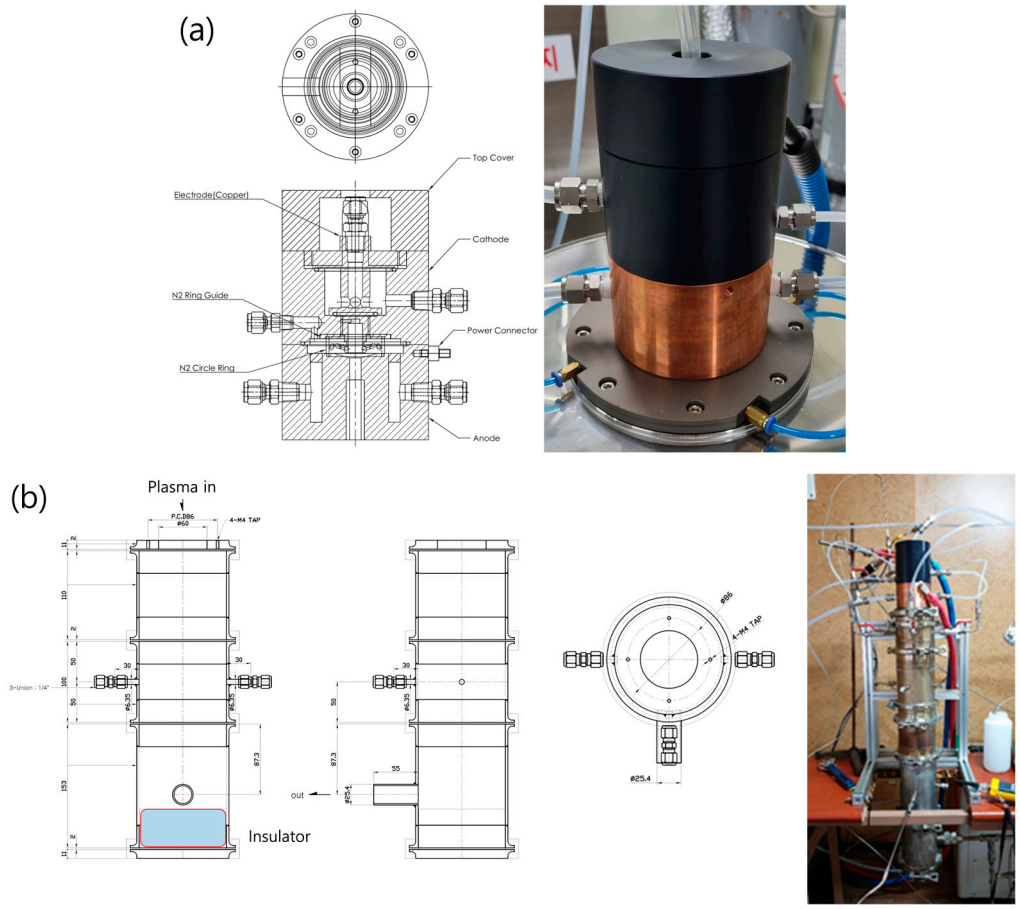


Figure 1. Schematic diagram of (**a**) the plasma torch and (**b**) the plasma chamber reactor.

The plasma supply system consists of a plasma torch, a plasma power supply, a plasma transfer gas supply, and a cooling water supply facility. For the plasma supply device, a non-transferred arc plasma torch was selected and manufactured at the 10 kW level for methane cracking at a feed rate of 1 to 10 L/min. Nitrogen gas was used as the plasma transfer gas to discharge the arc of the non-transferred plasma torch. In addition, a coolant circulation system was applied to cool the plasma electrode and the main body, and the thermal efficiency of the plasma torch could be evaluated by measuring changes in the coolant circulation flow rate and temperature.

The plasma chamber reactor was manufactured using stainless steel (STS-304) with a diameter of 60 mm to fit the plasma torch and a height of 480 mm based on the plasma flame length. The plasma torch was mounted at the top center of the reactor and the plasma flame was formed from top to bottom. To maintain parallel flows of plasma and reaction gas, the fuel inlet and product gas outlet were installed at the upper and lower sides of the reactor, respectively, to supply methane and discharge generated gas.

Methane was supplied in two ways, and the reaction characteristics based on the supply method were compared and evaluated. One way was to supply methane through a gas inlet installed on the upper side wall of the reactor (type A), and the other was to supply methane through a hybrid burner (Type B) located between the torch and the reactor, as shown in Figure 2.

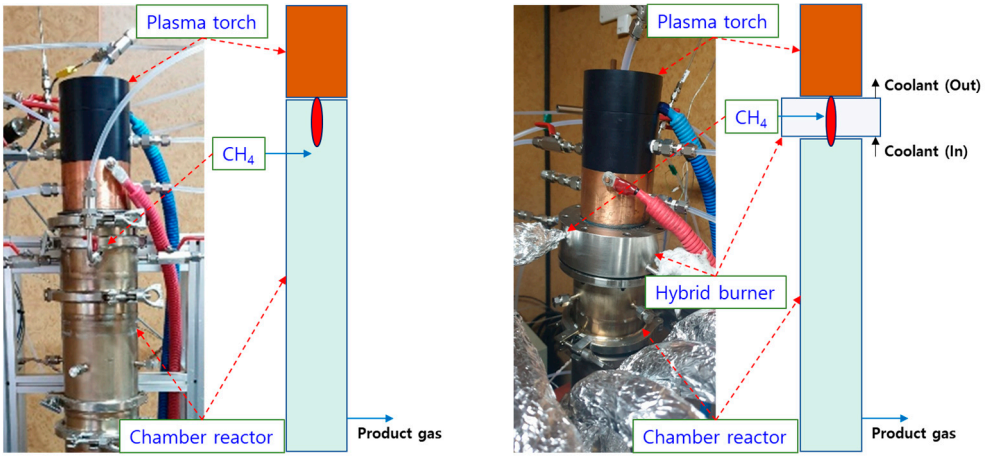


Figure 2. Comparison of methane supply methods of (**a**) type A and (**b**) type B.

Hybrid burners supplied methane close to the plasma flame by extending the methane supply line toward the center of the reactor. Additionally, cooling water was supplied to prevent damage to the methane supply lines due to a high-temperature plasma flame.

Thermocouples and pressure transmitters were installed to measure temperature and pressure changes inside the reactor and monitor the reaction status. In consideration of material deformation, a clamp-fastening method was applied to fix the cylindrical refractory in front of the gas outlet. After the plasma discharge was completed, the inside of the reactor was inspected to check for any abnormalities.

2.2. Instrumentation and Setup

The system for the arc plasma reaction experiment consisted of a gas supply section, a plasma reaction section, a cooling water circulation section, and a generated gas analysis section, as shown in Figure 3.

In the gas supply section, nitrogen gas (99% purity) for arc plasma discharge and methane (99.99% purity) for the reaction were supplied in fixed quantities via a mass flow controller (MFC, Brooks). First, the nitrogen supply was started, and then the plasma discharge was started while maintaining the nitrogen flow. When a stable plasma discharge state was confirmed, the reaction began by supplying methane.

The gaseous products from the methane plasma reactions were cooled and then discharged through a carbon capture filter (Teflon cartridge filter), and solid carbon particles generated during the reaction were captured by the filter (Figure 3c). The amount of solid carbon production was calculated by measuring the change in weight of the filter before and after the reaction. All weights of the filter were measured after the drying process. The carbon mass balance was calculated based on the amount of raw material fed and gas produced and the amount of carbon captured.

After passing through the carbon capture filter, the gases were analyzed in the gas analysis section. The contents of hydrogen and methane were checked in real time using an online IR gas analyzer (A&D system 2000, A&D system, Seoul, Republic of Korea) and an FTIR analyzer (C_1–C_4 analysis, Gasmet DX4000, Gasmet, Vantaa, Finland). At the same time, the product gas was sampled and further analyzed for its composition of C_1–C_5 hydrocarbons via GC (gas chromatography, YL6500, Young Lin, Anyang, Republic of Korea). In addition, the flow rate of the generated gas was measured using a dry gas meter, and all measured values were collected and stored in real time with a data logger (GL840, Graphtec, Yokohama, Japan) and used to organize the experimental results.

A detailed description of the experimental apparatus and methods can be found in the existing literature [14]. The main experimental variables and operating ranges of this study are summarized in Table 1.

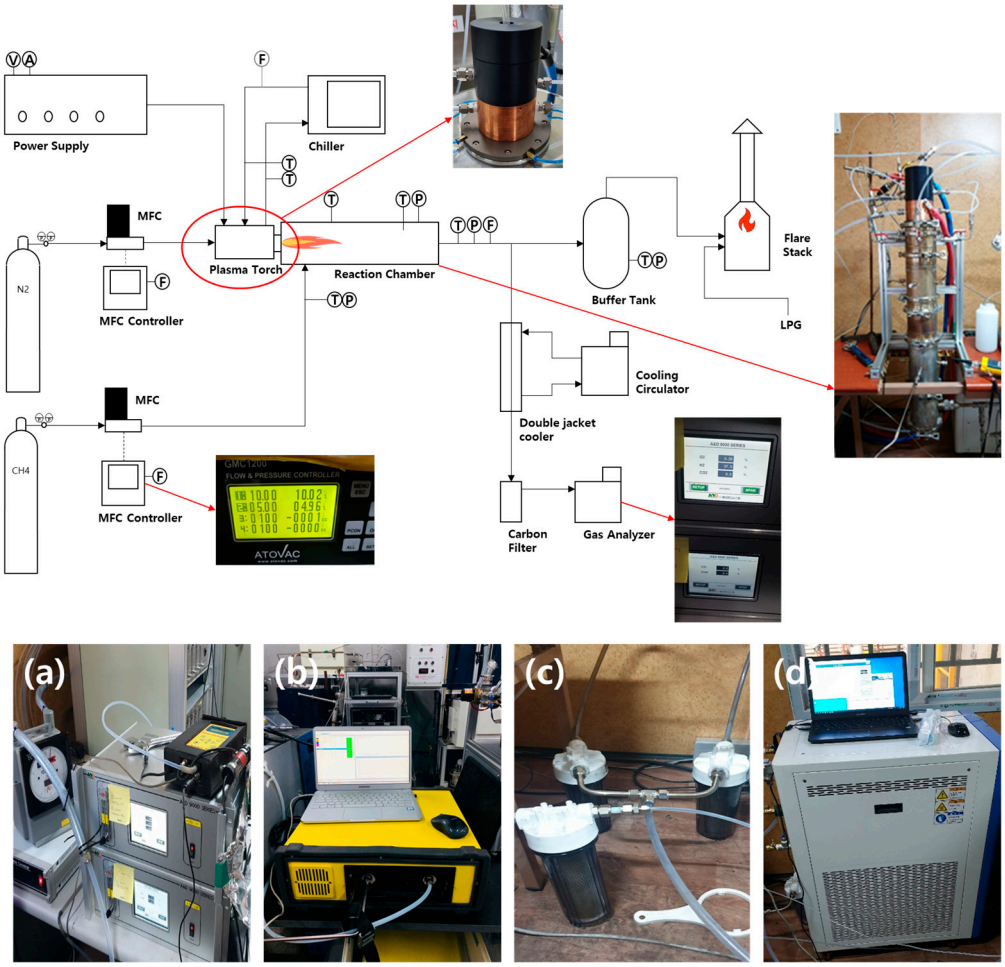


Figure 3. Schematic diagram of plasma reaction system and analyzer setup: (**a**) online IR analyzer and dry gas meter; (**b**) FTIR analyzer; (**c**) carbon filter; (**d**) cooling water supply.

Table 1. Experimental variables and operating ranges.

Variables		Unit	Operating Range
Methane	Supply method	-	Type A, B
	Feed rate	L/min	1–10
Nitrogen (plasma transfer gas) feed rate		L/min	8–10
Plasma	Current	A	15–20
	Voltage	V	100–200
	Power	kW	2–4

The main factors to evaluate the performance of the methane plasma reaction can be defined as follows.

$$\text{Thermal efficiency } (\eta_{Plasma}) = \frac{P_{Plasma} - Heat\ of\ cooling\ water}{P_{Plasma}} \times 100\%, \quad (1)$$

where η_{Plasma} and P_{plasma} represent plasma thermal efficiency and plasma power output, respectively.

$$\text{Conversion } (C_{CH4}) = \frac{Mass\ of\ methane\ supply - Mass\ of\ unreacted\ methane}{Mass\ of\ methane\ supply} \times 100\%, \quad (2)$$

$$\text{Yield of hydrogen } (Y_{H2}) = \frac{Moles\ of\ hydrogen\ production}{Moles\ of\ methane\ supply \times 2} \times 100\%, \quad (3)$$

$$\text{Yield of solid } carbon\ (Y_C) = \frac{Moles\ of\ solid\ carbon\ production}{Moles\ of\ methane\ supply} \times 100\%, \quad (4)$$

where the yield of each component is based on the theoretical production of 2 moles of hydrogen and 1 mole of carbon per mole of methane, as shown in the reaction equation above.

$$\text{Energy efficiency } (\eta_{Energy}) = \frac{\sum m_i \times LHV_i}{m_{Methane} \times LHV_{Methane} + P_{Plasma}} \times 100\%, \quad (5)$$

where η_{Energy} represents energy efficiency, which is the ratio of the energy of product i to the power energy supplied by plasma and the chemical energy supplied by methane. LHV and m refer to the lower heating value and mass flow rate of product i and methane, respectively.

3. Results

3.1. Characteristics of Plasma Discharge

Plasma discharge characteristics such as plasma flame stability, plasma power, power loss, and thermal efficiency can be affected by the applied current and plasma transfer gas flow rate. To avoid the effect of plasma discharge space limitation, the plasma discharge characteristics were investigated in an open space, and the formation of plasma flames based on the discharge conditions is compared in Figure 4.

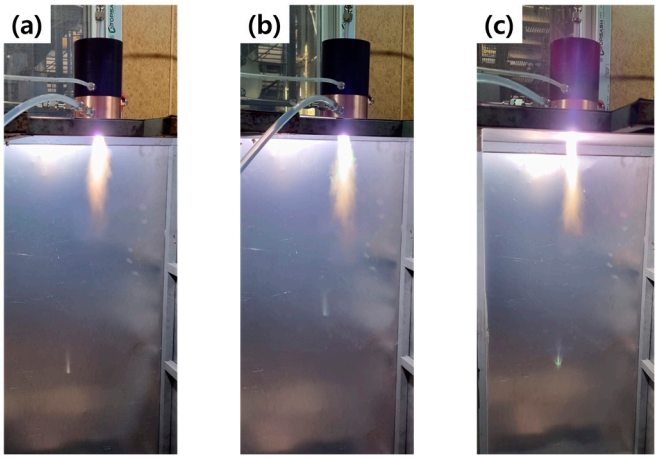


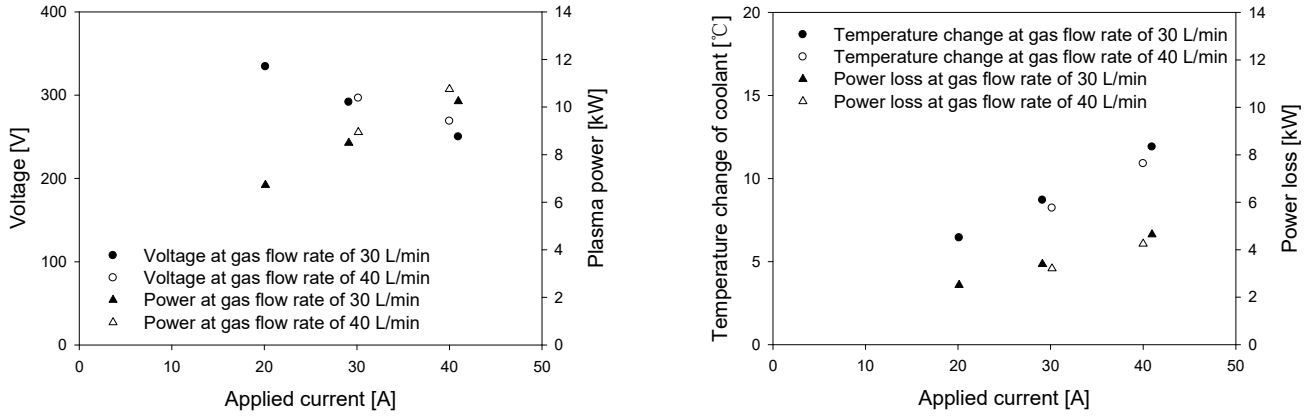
Figure 4. Comparison of plasma flames under applied currents and gas flow rates of (**a**) 20 A and 30 L/min, (**b**) 40 A and 30 L/min, and (**c**) 40 A and 40 L/min.

As can be seen from Figure 4a,b, under constant flow rate conditions, the formation of the plasma flame was found to become unstable as the applied current increased. However, as the flow rate increased (Figure 4b,c), the size of the flame increased, and it appeared to maintain a stable shape. Generally, under certain power conditions of plasma discharge, as the applied current increased, the plasma transfer gas flow rate decreased, and the plasma flame length decreased accordingly. The length of the flame affected the thermal shock of the plasma torch electrode, and as the length became shorter, the thermal shock tended to increase. On the other hand, as the voltage was maintained at a high level, the transfer gas flow rate increased and the length of the plasma flame increased accordingly, thereby alleviating the thermal shock to the electrode.

The effects of applied current on plasma discharge power and power loss under a constant gas flow rate are shown in Figure 5.

As the applied current increased from 20 A to 40 A, the voltage slightly decreased, but the plasma power increased from 6.7 kW to 10.2 kW at gas flow rate of 30 L/min and from 8.9 kW to 10.8 kW at gas flow rate of 40 L/min, thus reducing the overall plasma resistance. The reduction in plasma resistance is related to arc length and electrical conductivity. In this study, this can be understood as the effect of increasing electrical conductivity as

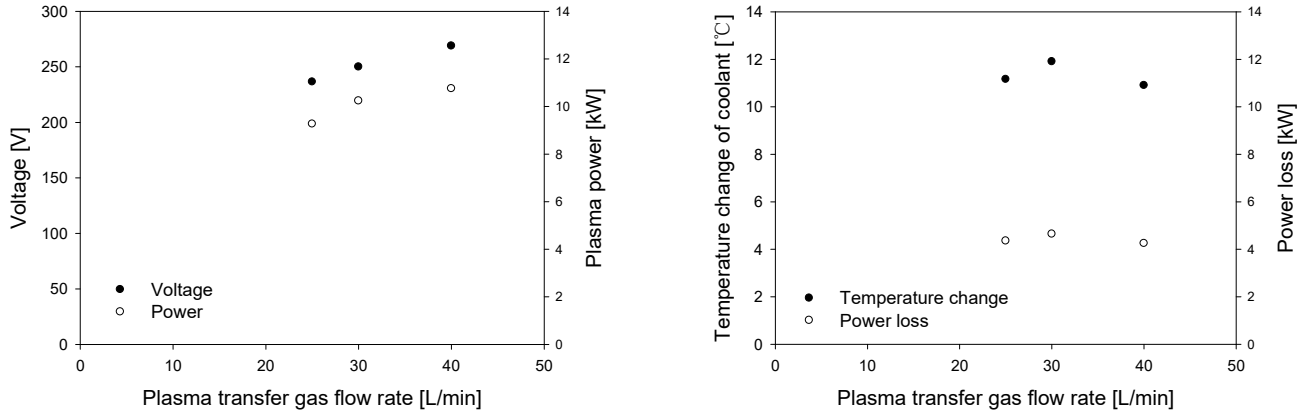
the temperature increased, and the arc length at the fixed electrode can be considered to have been relatively constant. Additionally, as the current increased, the coolant outlet temperature increased compared to the relatively constant coolant inlet temperature. In addition, as the difference between the coolant inlet and outlet temperatures increased, the power loss, that is, the heat loss due to cooling water, also increased from 2.5 kW to 4.6 kW, accounting for about 45% of the total plasma power.



(**a**) (**b**)

Figure 5. Effect of applied current on plasma discharge characteristics: (**a**) plasma voltage and power; (**b**) coolant temperature change and power loss.

In addition, Figure 6 shows the effect of the plasma transfer gas flow rate on the plasma power and power loss.



(**a**) (**b**)

Figure 6. Effect of plasma transfer gas flow rate on plasma discharge characteristics: (**a**) plasma voltage and power; (**b**) coolant temperature change and power loss.

As the plasma transfer gas flow rate increased, the voltage and plasma power tended to increase relatively linearly. However, the difference between the coolant inlet and outlet temperatures decreased, and heat loss due to the coolant also tended to decrease to about 40% of the total plasma power.

As a result, the thermal efficiency of the plasma discharge decreased from 62.6% to 54.6% as the applied current increased but increased from 53.0% to 60.4% as the gas flow rate increased (Figure 7).

This change in thermal efficiency of the plasma discharge is thought to have been due to the sensible heat transfer effect and the radiant heat transfer effect. As the plasma transfer gas flow rate increased, the sensible heat transfer effect of the gas increased, and as the flame length increased, the radiative heat transfer effect of the plasma flame increased, thereby

increasing the plasma thermal efficiency. On the other hand, whereas the thermal efficiency of previously reported large-capacity plasma torches reached the level of 70–90% [15,16], the thermal efficiency of this study using a 10 kW pilot plasma torch remained at a relatively low level of 53–64%. This is believed to have been because the heat loss due to the cooling system was relatively large for the small pilot torch, and additional tests are planned for mid- to large-sized facilities.

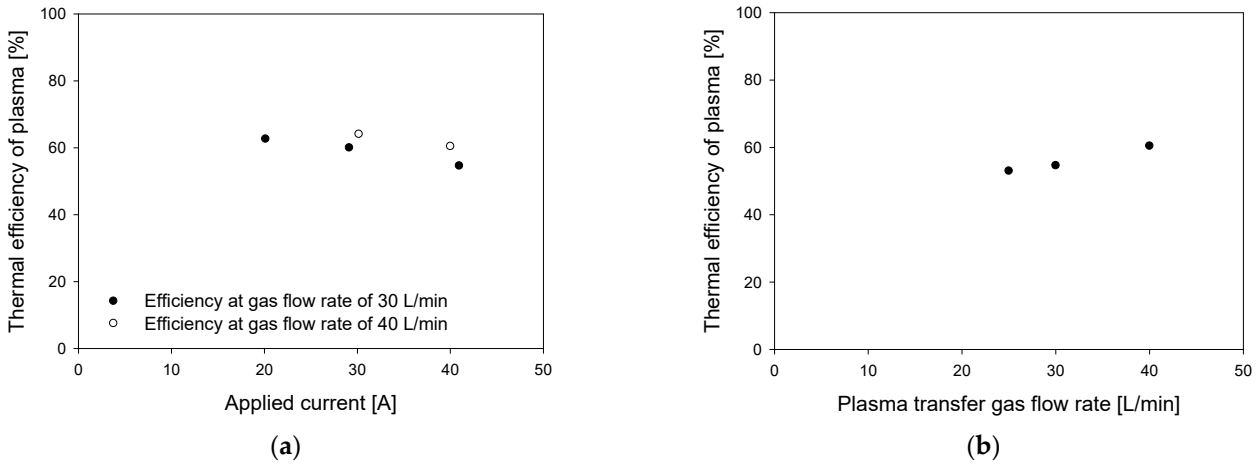


Figure 7. Thermal efficiency of plasma discharge based on (**a**) applied current and (**b**) plasma transfer gas flow rate.

3.2. Plasma Thermal Cracking of Methane

Methane thermal cracking experiments were carried out using two types of plasma reactors. As explained earlier, the only difference between the two reactors was the methane supply method, but the size of the reactors was the same. Figure 8 shows the typical plasma discharge operation and product gas composition using the type A reactor. The results using the type B reactor showed a similar trend.

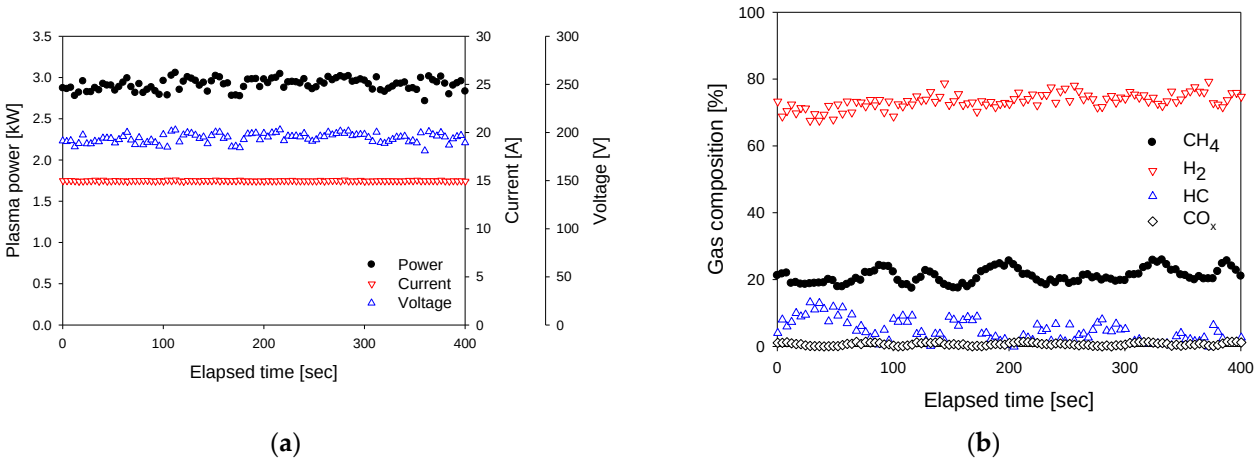


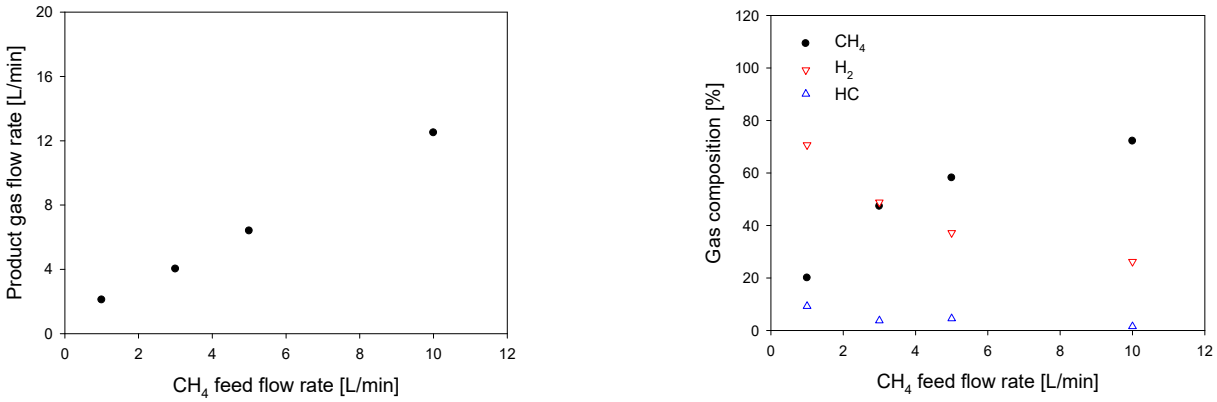
Figure 8. Online measurements of (**a**) plasma discharge operation and (**b**) product gas composition (N_2 free).

The plasma discharge output in the reaction chamber was reduced to about 2~4 kW due to space constraints, but it was confirmed that the discharge could be maintained stably. The gas generated during the methane thermal cracking process was cooled and then analyzed using an online IR gas analyzer. As the reaction progressed, the gas composition also remained relatively constant. In the case of small plasma facilities, the content of plasma transport gas is relatively large, and in this study, nitrogen as the plasma transport

gas accounted for about 80% of the reactor outlet gas. Therefore, the product gas was evaluated on a N_2-free basis. The product gas consisted mainly of hydrogen, accounting for about 70% on a N_2-free basis, and the remainder consisted of unreacted methane (about 20%, N_2 free) and hydrocarbons of C_2 and higher (about 10%, N_2 free). On the other hand, carbon oxides such as CO and CO_2 were rarely generated, and the average composition was less than 1.6%. As a result, it was confirmed that turquoise hydrogen could be produced through this process.

3.2.1. Effect of Methane Feed Rate

The effect of the methane feed rate on methane thermal cracking was investigated using a type A reactor under constant power conditions to exclude plasma flame mixing effects. The type A reactor, unlike the type B reactor, maintained a certain distance between the plasma flame and methane feed port to prevent damage to the feed port due to plasma flame disturbance based on the methane feed rate. The changes in the flow rate and composition of methane thermal cracking gas products with methane feed rate are shown in Figure 9 on a N_2-free basis.



(**a**) (**b**)

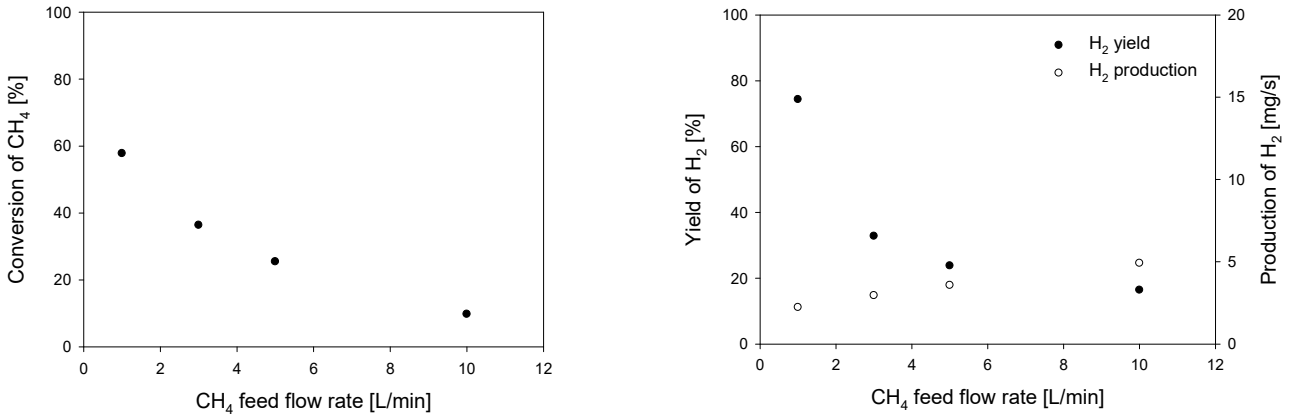
Figure 9. Changes in (**a**) product gas flow rate (N_2 free) and (**b**) product gas composition (N_2 free) as a function of CH_4 feed rate using plasma power controlled to within 3 to 3.5 kW.

As the methane feed rate increased, the product gas flow rate tended to increase relatively linearly due to the increased methane supply. On the other hand, the composition of the product gas indicates that the methane content increased, whereas the hydrogen content decreased as the methane feed rate increased. This is because the increased methane feed rate under constant plasma output conditions led to a relative decrease in reaction factors such as mixing and heat and mass transfer. As a result, unreacted methane increased, and the methane conversion decreased (Figure 10).

Methane conversion reached up to 57.8% at the low methane feed rate and decreased to 9.8% as the methane feed rate increased, which also reduced the hydrogen yield to 16.4%. However, hydrogen production increased due to an increased methane supply.

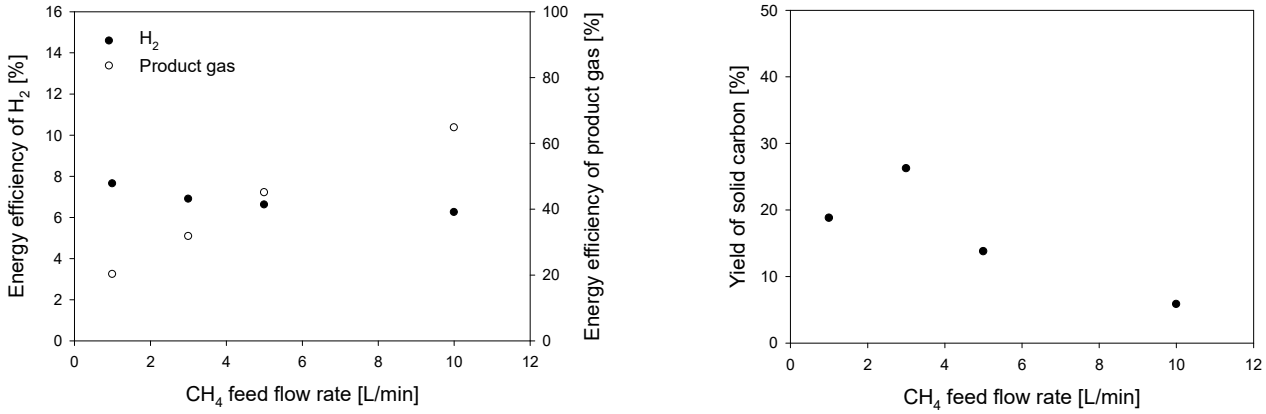
The effect of the methane feed rate on the energy efficiency of the hydrogen and gaseous product production is shown in Figure 11.

As the methane feed rate increased, the energy efficiency of the hydrogen production decreased slightly, with an average efficiency of approximately 6.8%. On the other hand, the energy efficiency of the product gas, including unreacted methane and other hydrocarbons, increased to approximately 65%. Energy loss resulted from sensible heat loss of the product gas and cooling water, as well as loss due to solid carbon production. Under constant plasma power conditions, the sensible heat loss can be maintained at a relatively constant level. However, as the methane feed rate increased, solid carbon production tended to decrease to around 5.8%, as shown in Figure 11b, and energy loss due to the solid carbon also tended to decrease accordingly.



(**a**) (**b**)

Figure 10. Changes in (**a**) CH_4 conversion and (**b**) H_2 yield and production as a function of CH_4 feed rate using plasma power controlled to within 3 to 3.5 kW.



(**a**) (**b**)

Figure 11. Changes in (**a**) energy efficiency of H_2 and product gas and (**b**) C(s) yield as a function of CH_4 feed rate using plasma power controlled to within 3 to 3.5 kW.

3.2.2. Effect of Plasma Power

The effect of plasma power on the methane thermal cracking reactions was investigated under constant methane supply conditions to exclude the effect due to changes in methane flow rate. To confirm the mixing effect as well as the thermal effect based on the plasma power, a type B reactor capable of supplying methane close to the plasma flame was used. The changes in flow rate and composition of methane thermal cracking gas products with plasma power are shown in Figure 12 on a N_2-free basis.

Under constant methane feed rate conditions of 3 L/min and 5 L/min, as the plasma power increased to 3.3 kW and 2.8 kW, the product gas flow rate increased slightly, averaging 4.0 L/min and 6.2 L/min, respectively, on a N_2-free basis. In addition, as the plasma power increased, the unreacted methane content in the product gas decreased, whereas the hydrogen content increased, reaching 84.9% and 57.1% on a N_2-free basis, respectively. The average content of the hydrocarbons above C_2 remained almost constant at approximately 9% and 18% on a N_2-free basis, respectively, depending on the methane feed rate. As with the results of a type A reactor, carbon oxides were also not detected in the gas produced from the methane thermal cracking reaction using a type B reactor.

The changes in methane conversion and hydrogen yield according to plasma power are shown in Figure 13.

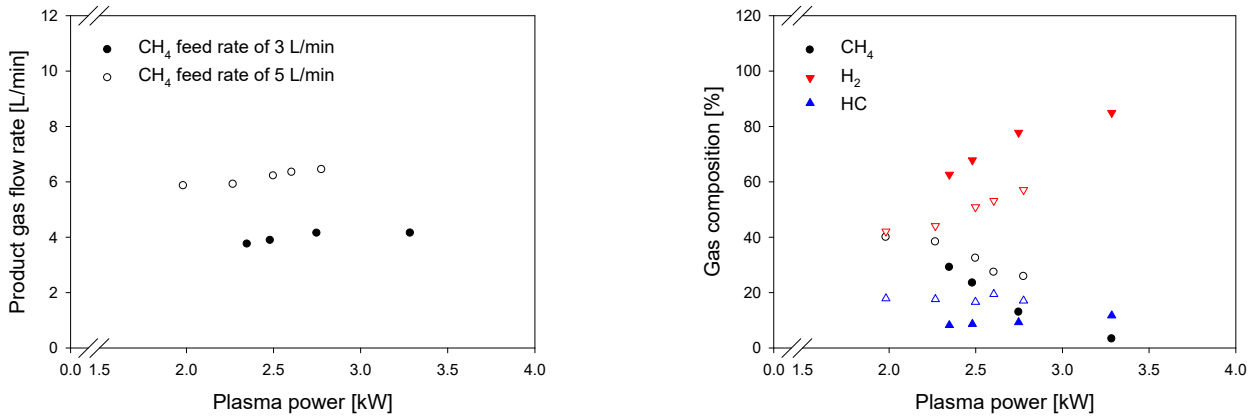


Figure 12. Changes in (**a**) product gas flow rate (N_2 free) and (**b**) product gas composition (N_2 free) as a function of plasma power at a CH_4 feed rate of 3 L/min (solid symbol) and 5 L/min (open symbol).

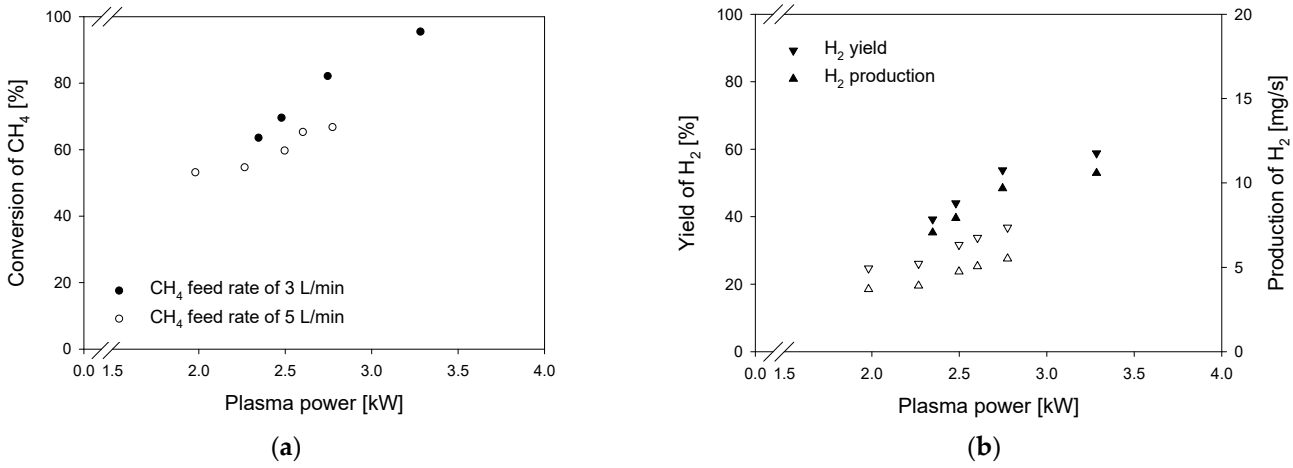


Figure 13. Changes in (**a**) CH_4 conversion and (**b**) H_2 yield and production as a function of plasma power at a CH_4 feed rate of 3 L/min (solid symbol) and 5 L/min (open symbol).

As the plasma power increased to 3.3 kW and 2.8 kW, the reduction in unreacted methane led to an increase in methane conversion to approximately 95% and 67% at the methane feed rates of 3 L/min and 5 L/min, respectively. In other words, as the plasma output increased by 40%, the methane conversion rate increased by 50% and 26% depending on the methane supply conditions, resulting in correlation coefficients of approximately 1.3 and 0.6, respectively. The increase in methane conversion is believed to have been due to improved mixing and heat and mass transfer effects as the plasma power increased. As a result, hydrogen production and yield also tended to increase.

Figure 14 shows the energy efficiency of the hydrogen and gaseous products production and the yield of solid carbon as a function of the plasma power.

As the plasma output increased to 2.7 kW, the energy efficiency of the hydrogen production tended to increase due to the increase in hydrogen production. However, when the plasma power increased to 3.3 kW, the increase in energy efficiency was offset by the increase in energy losses due to the increased energy supply, and thus the energy efficiency of hydrogen production stagnated or decreased slightly. On the other hand, the energy efficiency of gaseous products, including hydrogen, unreacted methane, and hydrocarbons, tended to decrease when increasing the plasma power, and it is believed to mainly have been due to the production of solid carbon. The increased methane conversion with increasing plasma power caused an increase in solid carbon yield, and the chemical energy and heat of the solid carbon was excluded from the energy efficiency evaluation.

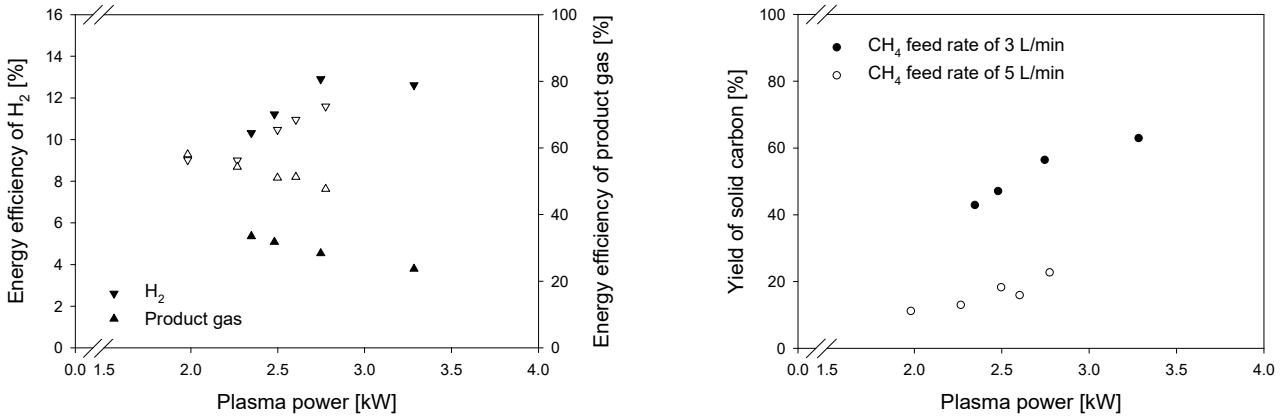


Figure 14. Changes in (**a**) energy efficiency of H_2 and product gas and (**b**) C(s) yield as a function of plasma power at a CH_4 feed rate of 3 L/min (solid symbol) and 5 L/min (open symbol).

3.2.3. Effect of Methane Supply Method

The effects of plasma flame mixing were examined by comparing the methane thermal cracking reaction characteristics based on the methane supply method under constant conditions of a methane supply amount of 3 L/min and a plasma output of 3.3 kW, and the main comparison results are summarized in Table 2.

Table 2. Comparison of the CH_4 thermal cracking characteristics between the type A and B reactors.

Characteristics	Type A	Type B	Ref [17]
Gas production (L/min, N_2 free)	4.0	4.2	-
CH_4 conversion (%)	36.4	95.4	5–96
CH_4 content (%, N_2 free)	47.4	3.3	-
H_2 content (%, N_2 free)	48.9	84.9	-
H_2 yield (%)	32.8	58.8	27–73
C(s) yield (%)	26.2	62.9	11–537 [(1)]

[(1)] C(s) yield in references is the ratio of carbon mass to catalyst mass.

Under the conditions of an almost identical plasma power and methane feed rate, the gas flow rate produced by the type B reactor was slightly increased compared to that of the type A reactor. On the other hand, as the unreacted methane decreased by 93%, the methane conversion in the type B reactor increased by more than twice that of the type A reactor. As a result, hydrogen and solid carbon yields increased by 79% and 140%, respectively. The improvement in reaction efficiency is believed to have been the result of rapid heat and mass transfer due to the high-temperature flow phenomenon by injecting the methane close to the plasma flame in the type B reactor compared to the type A reactor. Additionally, recent results from catalytic methane decomposition (CDM) processes are compared in Table 2. In the case of catalytic processes, the average value of recent results is compared because there is a large difference in conversion and yield depending on the type of catalyst used and operating conditions. The average methane conversion and hydrogen yield of the previous CDM processes were 64% and 50%, respectively, so the reaction efficiency of the type B reactor was evaluated as being relatively excellent. When the solid carbon productivity of the existing literature was adjusted according to Equation (4), the average carbon yield was about 51%, which is in a range similar to that of the results of this study.

In addition, the energy efficiency based on the total gas products and hydrogen production is compared to other processes in Table 3.

Table 3. Comparison of the energy efficiency of this study and other processes.

Technology	Energy Efficiency		Ref.
	Hydrogen	Total Gas	
This study (type A)	6.9%	31.8%	
This study (type B)	12.6%	23.7%	
Methane pyrolysis	58%		[18]
Thermochemical water splitting	20~45%		[19]
Water electrolysis	50~70%		[20]
Steam methane reforming	60% (with CCS)~75% (*w/o* CCS)		[18]
Plasma-assisted steam reforming	9~85%		[21]
Chemical looping steam reforming	65~75%		[21]
Biomass gasification	35~50%		[20]
Coal gasification	43% (with CCS)~60% (*w/o* CCS)		[5]

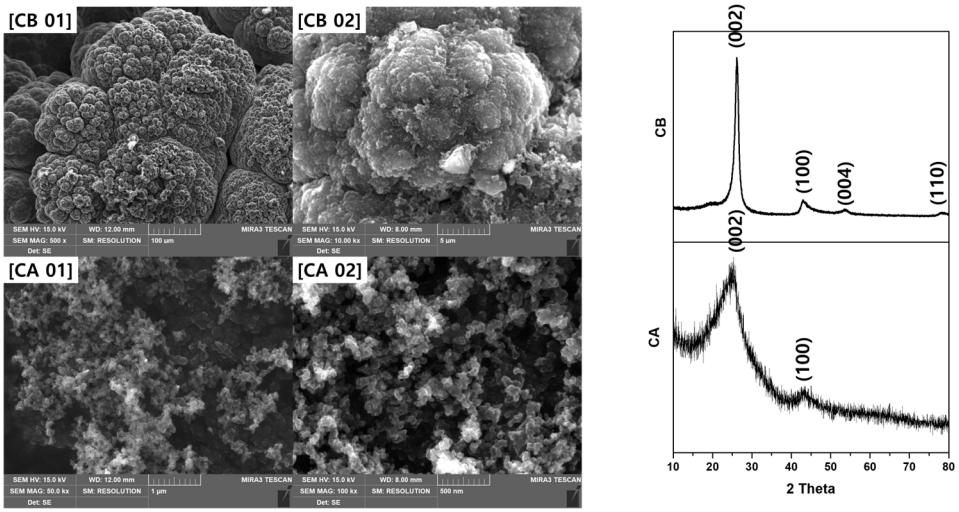
The energy efficiency of this study was evaluated as being relatively low compared to that of other processes such as water splitting and conventional conversion processes, and this is believed to mainly be the result of reduced plasma thermal efficiency and solid carbon production. As mentioned earlier, by using a small lab-scale plasma facility, the plasma thermal efficiency was found to be lower than that of a bench or demo-scale facility, and the heat losses can be reduced through process scale-up and optimal design.

In addition, the energy supplied through methane and plasma was converted and distributed into sensible heat and chemical energy of gas and solid products through the reactions. Unlike conventional processes that convert supplied carbon into gaseous products, this process recovers carbon components in the form of solid products. The solid carbon conserved approximately 13% (type A) and 31% (type B) of the raw material energy, which is consistent with previous findings [14]. Accordingly, the energy distribution of the gas product was reduced, and the energy efficiency of the generated gas was evaluated as low for the energy distributed in the solid carbon. As a result, the process can be made more competitive by converting solid carbon into high-value products.

3.3. Characteristics of Solid Carbon

The solid carbon generated by methane plasma thermal cracking reactions was recovered from the carbon filter of the downstream gas discharge line after completion of the reaction, and the carbon deposited on the inner wall was also be recovered after dismantling the reactor. The SEM image and XRD analysis results of the solid carbon recovered from the carbon filter (CA) and the carbon deposited on the inner wall near the plasma flame outlet (CB) are compared in Figure 15.

The carbon sample collected from the plasma flame outlet showed a more agglomerated form compared to the carbon sample recovered from the carbon filter. In addition, both of the solid carbon samples had a largely rounded shape with carbon nodules stuck together, like the morphology of fresh carbon black [22]. Additionally, as previously reported [23], high-purity carbon components were confirmed through SEM-EDX analysis of carbon samples. Meanwhile, the XRD analysis results showed different peak characteristics depending on sample recovery location. The results of carbon samples recovered from the plasma flame outlet (CB) showed sharper and more intense peaks compared to the peaks of carbon recovered from the reactor outlet, and these peak characteristics can be observed in carbon black that has undergone a high-temperature heat-treatment process [24]. Heat-treated carbon black can uniformly improve physical characteristics such as surface homogeneity, stability, and electrical resistance properties, which affect product quality and performance, so it can be used in a variety of fields [25].



(**a**) (**b**)

Figure 15. (**a**) SEM images and (**b**) XRD analysis of the solid carbon recovered at the reactor outlet (CA) and plasma flame outlet (CB).

4. Conclusions

In this study, methane thermal cracking experiments were carried out using a DC arc plasma torch. The main product of this process is turquoise hydrogen without CO_2 generation. In addition, solid carbon as a byproduct can also be used as a valuable chemical.

As a result of preliminary tests on the plasma discharge characteristics, it was possible to induce a stable operation by increasing the high voltage and plasma transfer gas flow rate, and it is believed that damage to the plasma electrode can be reduced under these conditions. In the methane thermal cracking experiments, stable discharge was confirmed by controlling the plasma power in the range of 2 to 4 kW. The experimental results show that the hydrogen yield decreased to 16.4% as the methane feed rate increased. On the other hand, under conditions where the methane feed rate was kept constant, the methane conversion increased with increasing plasma power, resulting in an increase in hydrogen yield to 58.8%. The yield of hydrogen and methane conversion was also greatly affected by the methane supply method. Under the condition of supplying methane close to the plasma flame, hydrogen yield and methane conversion increased by approximately 79% and 160%, respectively. In addition, the change in solid carbon yield based on the methane feed rate and plasma power showed a similar trend to the hydrogen yield, and the solid carbon yield was also found to increase to 62.9% under the condition of maximum hydrogen yield.

Solid carbon materials are used for various purposes in various fields, such as the rubber industry, the ink and paint industry, electrical conductors, the plastic and textile industry, etc. Through this process, high-purity solid carbon can be recovered, and carbon with high-temperature heat treatment characteristics can also be recovered in the plasma flame area. Additionally, the recovered carbon can be used to manufacture graphene, which is used as a high-tech industrial material, via further purification and upgrading processes. As a result, with process optimization based on the intended use of the final product, it is possible to produce not only clean hydrogen but also high-purity solid carbon that has various uses as a chemical product. Commercialization of recovered carbon is as important as producing and utilizing clean hydrogen, which can strengthen the competitiveness of this process compared to existing processes.

Author Contributions: Conceptualization, D.-K.P. and J.-H.R.; methodology, D.-K.P. and J.-H.R.; formal analysis, D.-K.P.; investigation, D.-K.P., S.-N.P., H.-J.K., H.-S.K., J.-H.K. and J.-H.R.; data curation, D.-K.P. and J.-H.K.; writing—original draft preparation, D.-K.P. and J.-H.R.; writing—review and editing, D.-K.P. and J.-H.R.; visualization, D.-K.P.; project administration, J.-H.R.; funding acquisition, J.-H.R. All authors have read and agreed to the published version of the manuscript.

Funding: This study is the result of a study conducted with support from the Korea Technology and Information Promotion Agency with funding from the Ministry of SMEs and Startups in 2022 (No. RS-2022-00165632).

Data Availability Statement: The data presented in this study are available on request from the corresponding author. The data are not publicly available due to the funding institution's research security pledge.

Conflicts of Interest: The authors declare no conflicts of interest.

References

1. Kim, S. The concept and justification of carbon neutrality. *Monthly Elec. J.* **2021**, *1*, 18–24.
2. IEA. *World Energy Statistics 2019*; IEA: Paris, France, 2019.
3. Diab, J.; Fulcheri, L.; Hessel, V.; Rohani, V.; Frenklach, M. Why turquoise hydrogen will be a game changer for the energy transition. *Int. J. Hydrogen Energy* **2022**, *47*, 25831–25848. [CrossRef]
4. Arcos, J.M.M.; Santos, D.M. The Hydrogen Color Spectrum: Techno-Economic Analysis of the Available Technologies for Hydrogen Production. *Gases* **2023**, *3*, 25–46. [CrossRef]
5. Sánchez-Bastardo, N.; Schlögl, R.; Ruland, H. Methane Pyrolysis for Zero-Emission Hydrogen Production: A Potential Bridge Technology from Fossil Fuels to a Renewable and Sustainable Hydrogen Economy. *Ind. Eng. Chem. Res.* **2021**, *60*, 11855–11881. [CrossRef]
6. Ekona's Tri-Generation Pyrolysis (TGP) Solution for Blue Hydrogen Production. December 2019. Available online: https://arpa-e.energy.gov/sites/default/files/4%20Ekona.pdf (accessed on 11 November 2022).
7. Schneider, S.; Bajohr, S.; Graf, F.; Kolb, T. State of the Art of Hydrogen Production via Pyrolysis of Natural Gas. *ChemBioEng Rev.* **2020**, *7*, 150–158. [CrossRef]
8. Fulcheri, L.; Rohani, V.J.; Wyse, E.; Hardman, N.; Dames, E. An energy-efficient plasma methane pyrolysis process for high yields of carbon black and hydrogen. *Int. J. Hydrogen Energy* **2023**, *48*, 2920–2928. [CrossRef]
9. Garduño, M.; Pacheco, M.; Pacheco, J.; Valdivia, R.; Santana, A.; Lefort, B.; Estrada, N.; Rivera-Rodríguez, C. Hydrogen production from methane conversion in a gliding arc. *J. Renew. Sustain. Energy* **2012**, *4*, 021202. [CrossRef]
10. Conrads, H.; Schmidt, M. Plasma generation and plasma sources. *Plasma Sources Sci. Technol.* **2000**, *9*, 441–454. [CrossRef]
11. Fridman, A. *Plasma Chemistry*; Cambridge University Press: Cambridge, UK, 2008.
12. Lynum, S.; Hox, K.; Haugsten, K.E.; Langoy, J. System for the Production of Carbon Black. International Patent WO 93/21053, 14 October 1993.
13. Harrison, S.B. sbH4 Consulting. Available online: www.digitalrefining.com (accessed on 16 November 2022).
14. Park, D.K.; Kim, J.H.; Kim, H.S.; Kim, J.H.; Ryu, J.H. Possibility Study in CO_2 Free Hydrogen Production Using Dodecane ($C_{12}H_{26}$) from Plasma Reaction. *Energies* **2023**, *16*, 1589. [CrossRef]
15. Chen, L.; Pershin, L.; Mostaghimi, J. A new highly efficient high-power DC plasma torch. *IEEE Trans. Plasma Sci.* **2008**, *36*, 1068–1069. [CrossRef]
16. Rutberg, P.G.; Safronov, A.A.; Popov, S.D.; Surov, A.V.; Nakonechny, G.V. Investigation of Voltage and Current Variations in a Multiphase AC Electric Arc System. In Proceedings of the 12th International Congress on Plasma Physics, Nice, France, 25–29 October 2004; pp. 25–29.
17. Korányi, T.I.; Németh, M.; Beck, A.; Horváth, A. Recent advances in methane pyrolysis: Turquoise hydrogen with solid carbon production. *Energies* **2022**, *15*, 6342. [CrossRef]
18. Steinberg, M. Fossil Fuel Decarbonization Technology for Mitigating Global Warming. *Int. J. Hydrogen Energy* **1998**, *24*, 771–777. [CrossRef]
19. Pinsky, R.; Sabharwall, P.; Hartvigsen, J.; O'Brien, J. Comparative review of hydrogen production technologies for nuclear hybrid energy systems. *Prog. Nucl. Energy* **2020**, *123*, 103317. [CrossRef]
20. Kalamaras, C.M.; Efstathiou, A.M. Hydrogen production technologies: Current state and future developments. *Conf. Pap. Energy* **2013**, *2013*, 690627. [CrossRef]
21. Das, A.; Peu, S.D. A Comprehensive Review on Recent Advancements in Thermochemical Processes for Clean Hydrogen Production to Decarbonize the Energy Sector. *Sustainability* **2022**, *14*, 11206. [CrossRef]
22. Lee, E.K.; Lee, S.Y.; Han, G.Y.; Lee, B.K.; Lee, T.J.; Jun, J.H.; Yoon, K.J. Catalytic decomposition of methane over carbon blacks for CO_2-free hydrogen production. *Carbon* **2004**, *42*, 2641–2648. [CrossRef]
23. Daghagheleh, O.; Schenk, J.; Zarl, M.A.; Lehner, M.; Farkas, M.; Zheng, H. Feasibility of a Plasma Furnace for Methane Pyrolysis: Hydrogen and Carbon Production. *Energies* **2024**, *17*, 167. [CrossRef]
24. Jurkiewicz, K.; Pawlyta, M.; Burian, A. Structure of carbon materials explored by local transmission electron microscopy and global powder diffraction probes. *C* **2018**, *4*, 68. [CrossRef]
25. Yoon, S.R.; Lee, J.K.; Cho, W.I.; Baek, Y.S.; Ju, J.B.; Cho, B.W. An electrochemical study on the carbon black conductor prepared by plasma pyrolysis of methane. *J. Korean Electrochem. Soc.* **2003**, *6*, 6–12.

Disclaimer/Publisher's Note: The statements, opinions and data contained in all publications are solely those of the individual author(s) and contributor(s) and not of MDPI and/or the editor(s). MDPI and/or the editor(s) disclaim responsibility for any injury to people or property resulting from any ideas, methods, instructions or products referred to in the content.